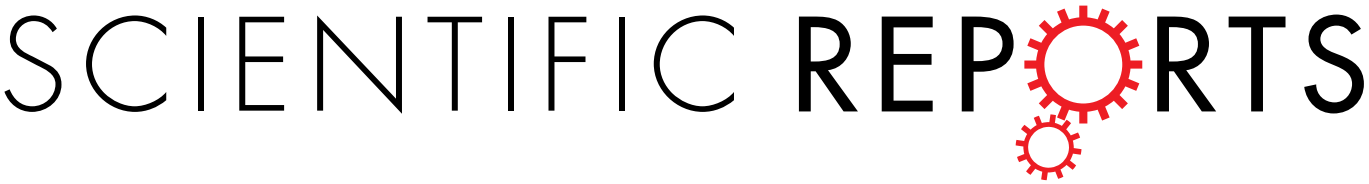

OPEN

Electrical synapses between inhibitory neurons shape the responses of principal neurons to transient inputs in the thalamus: a modeling study

Received: 1 November 2017
Accepted: 2 May 2018
Published online: 17 May 2018

Tuan Pham & Julie S. Haas

As multimodal sensory information proceeds to the cortex, it is intercepted and processed by the nuclei of the thalamus. The main source of inhibition within thalamus is the reticular nucleus (TRN), which collects signals both from thalamocortical relay neurons and from thalamocortical feedback. Within the reticular nucleus, neurons are densely interconnected by connexin36-based gap junctions, known as electrical synapses. Electrical synapses have been shown to coordinate neuronal rhythms, including thalamocortical spindle rhythms, but their role in shaping or modulating transient activity is less understood. We constructed a four-cell model of thalamic relay and TRN neurons, and used it to investigate the impact of electrical synapses on closely timed inputs delivered to thalamic relay cells. We show that the electrical synapses of the TRN assist cortical discrimination of these inputs through effects of truncation, delay or inhibition of thalamic spike trains. We expect that these are principles whereby electrical synapses play similar roles in regulating the processing of transient activity in excitatory neurons across the brain.

It is well known that thalamocortical (TC) neurons relay sensory information to the cortex. For example, sensory information from rodent whiskers is projected from trigeminal nuclei to the ventroposteromedial (VPM) nuclei and posteromedial (POm) nuclei in the ventrobasal (VB) complex of the thalamus[1,2]. From VPM and POm, afferent connections relay information about whisking to the barrels of the primary somatosensory cortex[3]. Within each of these nuclei, whisker inputs are encoded by varied latencies or spike rates[4,5].

During thalamocortical sensory relay, TC neuronal activity is regulated by a sheet of GABAergic neurons in the thalamic reticular nucleus (TRN)[6]. Most neurons within the ventrobasal complex (VB) receive monosynaptic GABAergic inputs from TRN neurons[7], and there is strong monosynaptic excitation from VB to TRN[8–10]. These reciprocal excitatory-inhibitory connections between TC and TRN neurons are likely to affect TC spiking, and the information relay from TC to cortex. For instance, large GABAergic conductances from TRN neurons have been shown to diminish information transfer in both computational models[11] and hybrid circuits of a model TRN – biological TC pair[12].

Although TRN neurons are homogeneously GABAergic, the prevailing evidence suggests that intra-TRN inhibition is not prevalent in adult mice[13]. At the microcircuit level, GABAergic synapses are reported at less than 1% of nearby TRN pairs[14]. The dominant source of intra-TRN connectivity, at least between nearby neurons, is thus electrical coupling via connexin36 (Cx36) gap junctions[14]. Hence, sensory information relay to cortical neurons from TC neurons is regulated by both GABAergic feedback inhibition from TRN neurons and the electrical synapses between them.

Electrical synapses have been widely reported to participate in the generation of synchronous or phase-locked neuronal activity[15]. This role has been confirmed through models of networks with embedded electrical synapses[16–18]. Within thalamocortical circuits, electrical synapses of the TRN help to synchronize the spindle

Department of Biological Sciences, Lehigh University, Bethlehem, PA, USA. Correspondence and requests for materials should be addressed to J.S.H. (email: julie.haas@lehigh.edu)

rhythms associated with slow-wave sleep or absence epilepsy[19,20]. However, the role of electrical synapses in TRN on the transient, stimulus-evoked TC activity is relatively underexplored.

Here we examine the role of electrical synapses within TRN on the activity patterns of TC neurons. We use a reduced model of four cells: two pairs of reciprocally connected TC-TRN neurons, with an electrical synapse between the two TRN neurons. We deliver closely-timed inputs, mimicking inputs of similar temporal, spatial, or frequency arriving from sensory surround, to the TC cells. We examine how TC spiking is impacted by the inhibition delivered from the coupled TRN neurons. Our results demonstrate that electrical synapses can either fuse or further separate input-generate spiking, and we predict that these effects ultimately impacting the ability of recipient cortical cells to discriminate between the inputs.

Methods

Model and simulations. Our model is based on a Hogkin-Huxley formalism for single compartmental model of TRN neurons[21] (Eq. 1).

$$\begin{aligned} C_m\frac{dV_i}{dt} &= (E_{lk}-V_i)\times g_{lk} + \sum_{\substack{ion\\channels}}(E_{chn}-V_i)\times g_{chn}(t) \\ &+ \sum_{\substack{chemical\\synapses}}^{j\neq i}\left(E_{syn}-V_i\right)\times g_{syn}\left(t,\ t_j^{events}\right) + \sum_{\substack{electrical\\synapses}}^{j\neq i}\left(V_j-V_i\right)\times g_{elec,ji} \\ &+ \sum_{\substack{external\\inputs}}\left(E_{syn}-V_i\right)\times g_{syn}(t,\ t_{external}^{events}) \end{aligned} \tag{1}$$

We used C_m of 1 µF/cm^2. Ionic currents ($\overline{G}_{chn}$, E_{chn}) include fast transient Na^+ current (60.5 mS/cm^2, 50 mV); K^+ delayed rectifier (60 mS/cm^2, −100 mV); K^+ transient A current (5 mS/cm^2, −100 mV); slowly inactivating K-current K2 (0.5 mS/cm^2, −100 mV); slow anomalous rectifier (H current) (0.025 mS/cm^2, −40 mV); low threshold transient Ca^{2+} current (T current) (0.67 mS/cm^2, 125 mV); leak current (0.06 mS/cm^2, −75 mV). The membrane voltage initial condition ($V_0 = -70.6837$ mV) was found by looking for the steady state after a simulation of 5000 ms.

Chemical synapses include fast inhibitory $GABA_A$ ($E_{GABA} = -75\,mV$) and excitatory AMPA ($E_{AMPA} = 0\,mV$) synapses. Synaptic conductance kinetics is implemented with a pair of fall and rise time constants (with $\tau_{rise} = 0.1\tau_{fall}$ for both synapses); $\tau_{fall,GABA} = 5\,ms$ and $\tau_{fall,AMPA} = 2\,ms$. Implementation of synapses resembles NEURON's implementation of[22] from ModelDB. (Eqs 2 and 3).

$$\begin{cases} t_{peak} = \dfrac{\tau_{fall}\times\tau_{rise}}{\tau_{fall}-\tau_{rise}}\ln\dfrac{\tau_{fall}}{\tau_{rise}} \\ f_s = \dfrac{\tau_{fall}}{-e^{1-\frac{t_{peak}}{\tau_{rise}}}+e^{1-\frac{t_{peak}}{\tau_{fall}}}} \end{cases} \quad (Normalization\ factor) \tag{2}$$

$$\begin{cases} g(t) = \overline{g}\times(B-A) \\ \dfrac{dB}{dt} = \dfrac{B+f_s\times w}{\tau_{fall}} \\ \dfrac{dA}{dt} = \dfrac{A+f_s\times w}{\tau_{rise}} \\ w = \sum_{spikes} H(t-t_k) \end{cases} \quad (Chemical\ synpase\ kinetics) \tag{3}$$

t_k: time of k^{th} event

$$H(x) = \begin{cases} 0\ if\ x<0 \\ 1\ if\ x\geq 0 \end{cases}$$

Our simulated network consists of 2 TRN cells connected via a single electrical synapse, and 2 TC cells receiving external input (Fig. 1A), simulated for 250 ms. Within the network, TRN cells each send inhibitory input to TC cells via $GABA_A$ synapses, and TC cells send excitatory inputs to TRN cells via AMPA synapses. Since the model was easily excitable, no additional DC current was sent to TRN neurons to reach subthreshold excitation. External inputs are AMPAergic excitatory inputs and provided only to the two TC cells.

Model electrical synapses (gap junctions) are linear and symmetrical. Values of electrical synapse conductance (G_{elec}) varied from 0 to 0.025 mS/cm^2, which converts to a coupling coefficient of roughly 0.2883. An applied current, iDC, was used from 0 to −0.1 µA/cm^2 to quantify membrane conductance $G_m \approx 0.0551$ mS/cm^2 and the effective coupling coefficient values, which do not differ significantly with the theoretical values of $G_m/(G_m+G_{elec})$ (data not shown).

The maximal GABAergic conductance (G_{GABA}) varied from 0 to 0.05 mS/cm^2, and the maximal AMPAergic conductance (G_{AMPA}) between TC and TRN cells was fixed at 0.05 mS/cm^2 to make sure that at least two spikes

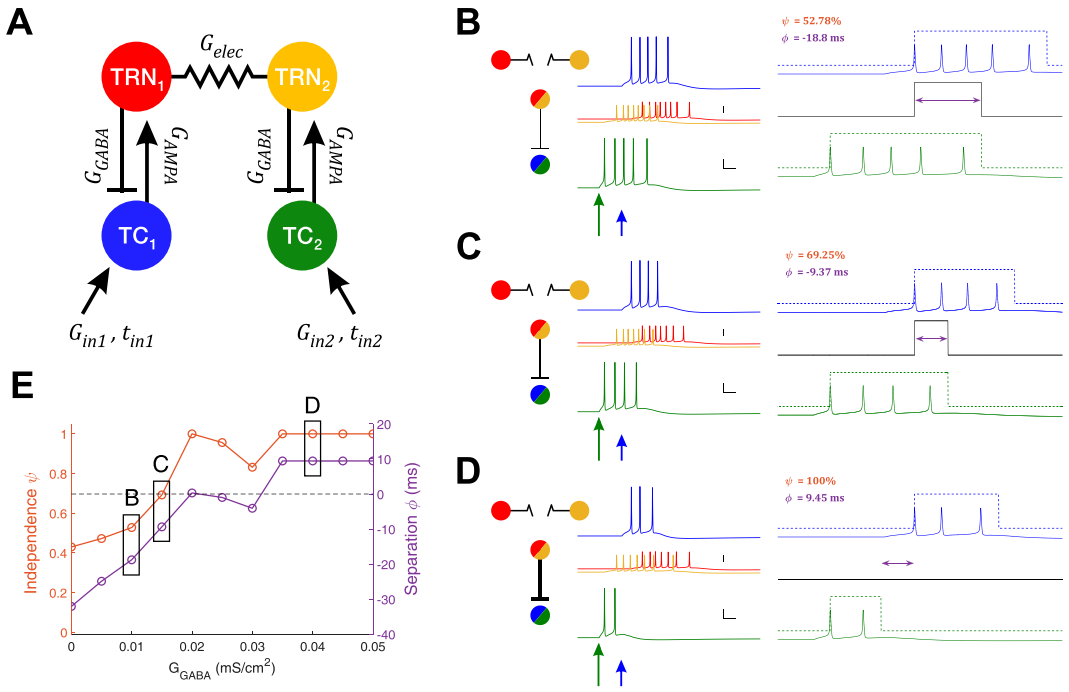

Figure 1. Model schematic and results with no electrical synapse. (**A**) Model is composed of two sets of TRN and TC cells, with reciprocal chemical synaptic connections between pairs, and one electrical synapse between the two TRN cells. Each simulation of the model used different values of connection strengths G_{elec}, G_{GABA} and input to TC_2, G_{in2} and t_{in2}. (**B**,**C**,**D**) Simulation examples, each with $G_{elec} = 0$, and input to TC_2 (green arrow) was large and early ($G_{in2} = 0.09$ mS/cm^2, $t_{in2} = 40$ ms). Input to TC_1 was constant (0.06 mS/cm^2, 60 ms). Over the three simulations shown, inhibitory synapses increased in strength ($G_{GABA} = 0.010$, 0.015, 0.040 mS/cm^2 respectively). In each subpanel, on the left are voltage traces color-coded as in (**A**), with the TRN traces superimposed and vertically reduced. Scale bars for TC traces are 20 mV, 10 ms; vertical scale bar of TRN traces is 40 mV. TC traces are expanded on the right, to demonstrate the computations for TC independence ψ and separation ϕ. Dotted lines represent the spiking window used to compute independence and separation. The black solid line indicates the amount of temporal overlap of TC spiking windows; purple arrows indicate the amount of temporal separation or overlap. (**E**) Independence (orange) and separation (purple) shown for this input over all values of G_{GABA}, with letters indicating the examples shown in (**B**,**C** and **D**). The dashed black line marks the transition from overlapping spike trains (negative separation) and completely independent spike trains (positive separation).

from a TC cell were required to elicit response from a TRN cell in an uncoupled network. External input to TC_1 (in) stays constant at maximal conductance (G_{in1}) of 0.06 mS/cm^2, and arrives (t_{in1}) at 60 ms. The arrival times (t_{in2}) of external input to TC_2 (in_2) varied between 10 and 110 ms. The maximal conductance (G_{in2}) of the input to TC_2 varied from 0.02 to 0.1 mS/cm^2.

Each simulation was simulated in parallel using MATLAB R2016 Parallel Toolbox and Lehigh University High Performance Computing Resources (Sol), solved with MATLAB's *ode23* Runge-Kutta implementation using a maximum timestep of 0.01 ms.

Analysis. For each simulation, the number of spikes in each TC neuron was extracted. Temporal independence (ψ) and spiking separation (ϕ) were defined as outlined below.

Thalamocortical spiking window and normalized temporal independence. The spiking window (σ) of a neuron was defined to be the temporal duration between its first spike and last spike, with addition of a 5-ms window following the last spike used to allow for EPSP decay in a cortical cell (Eq. 4). If a neuron does not fire, its spiking window is considered to be empty ($|\sigma_i| = 0$).

$$Spiking\ Window\ of\ TC_i\text{: } \sigma_i = [t_i^{(1)},\ t_i^{(end)} + 5] \tag{4}$$

From each TC spike train, relative independence of the corresponding TC (Eqs 5 and 6) was calculated and normalized to values between 0 (complete overlap) and 1 (no overlap) as described in the following equations. If either of TC neurons does not spike, we consider them to be completely independent (Eq. 6*).

$$Independence\ of\ TC_i\text{:}\ \ \psi_i = 1 - \frac{|\sigma_1 \cap \sigma_2|}{|\sigma_i|} \tag{5}$$

$$Independence\ of\ TC\text{:}\ \ \psi = \sqrt{\frac{\psi_1^{\,2} + \psi_2^{\,2}}{2}} \tag{6}$$

$\psi, \psi_i \in [0, 1]$; *if* $|\sigma_1| \times |\sigma_1| = 0 \rightarrow \psi = \psi_1 = \psi_2 = 1$; $[a, b]$: *Time interval between a, b*; $|x|$: *length of x*

Thalamocortical temporal separation. The separation of TC_1 and TC_2 spike trains (Eq. 7) was computed as the time difference between the spiking window termination of the leading neuron and the spiking window beginning of the following neuron. Separation is considered to be positive when both TCs spike and are independent of each other (Eq. 7a). In overlapping cases, this measure is artificially set as negative, as loss of separation, with the magnitude as the temporal amount of overlap (Eq. 7b). In cases of either TC_1 or TC_2 not spiking, this measure is undefined (Eq. 7c).

$$\phi_{\mathrm{dur}} = \begin{cases} +\left\|\max \sigma_{lead},\ \min \sigma_{follow}\right\| & if\ \psi = 1\ and\ |\sigma_1| \times |\sigma_2| > 0 \quad (a) \\ -|\sigma_1 \bigcap \sigma_2| & if\ \psi < 1 \quad (b) \\ NaN & if\ |\sigma_1| \times |\sigma_2| = 0 \quad (c) \end{cases} \tag{7}$$

Gain in independence and temporal separation. For each pair of (G_{elec}, G_{GABA}) we represented independence (or separation) in the parameter space of input differences between in_2 and in_1 $\left(\Delta_{\substack{Input \\ strength}} = \Delta G_{in} = G_{in2} - G_{in1},\ \Delta_{\substack{Input \\ timing}} = \Delta t_{in} = t_{in2} - t_{in1}\right)$. We denote this representation as $\psi_{\Delta in}(G_{elec},\ G_{GABA})$ or $\phi_{\Delta in}(G_{elec},\ G_{GABA})$.

For each pair $(G_{elec} \neq 0, G_{GABA})$, we calculated the gain in independence (or separation) as the difference of the quantitative measure from its value in the uncoupled case ($G_{elec} = 0$) for each G_{GABA}. In other words, the representation becomes $Gain[\psi_{\Delta in}(a \neq 0,\ b)] = \psi_{\Delta in}(a,\ b) - \psi_{\Delta in}(0,\ b)$ or $Gain[\phi_{\Delta in}(a \neq 0,\ b)] = \phi_{\Delta in}(a,\ b) - \phi_{\Delta in}(0,\ b)$.

In the input difference space, for each pair $(\Delta G_{in},\ \Delta t_{in})$, we calculated a normalized combination for input differences as $r_{\substack{input \\ diff}} = \sqrt{\left(\frac{\Delta G_{in}}{\max \Delta G_{in}}\right)^2 + \left(\frac{\Delta t_{in}}{\max \Delta t_{in}}\right)^2}$ and divided them into 5 strata. We then computed gain for each input difference combination, with non-negative gains shown on the top semi-arcs and non-positive gains shown on the bottom semi-arcs. For separation, undefined (NaN) values (refer to Eq. 7c) that arise from one neuron failing to spike are represented visually as missing values.

Results

To examine the impact of electrical synapses of the TRN on thalamocortical transmission, we constructed a 4-cell model comprising two pairs of reciprocally connected TC and TRN cells, with an electrical synapse between the two TRN cells (Fig. 1A). We used values of G_{elec} from zero to 0.025 mS/cm^2, corresponding to coupling coefficients measured in our model TRN neurons ranging from 0 to 0.3, mimicking the physiological range of cc values in TRN[14,23]. Input delivered to TC_1 was fixed at a constant arrival time and strength, and the inputs to TC_2 were varied in arrival time and input strength. We used input strengths that resulted in a burst of spikes that is typical of thalamic cells, lasting for tens of ms (e.g. Fig. 1B). To characterize the impact of electrical synapses on the output of the TC cells, we quantified independence (ψ) as the percentage as inversely related to the temporal intersection of the two TC spike trains, normalized to the duration of spiking. We also quantified separation (ϕ) as the time interval between the termination of one spike train and the onset of spiking in the other TC cell; negative values of separation result from overlapping trains. Higher values of independence and positive values of separation, we believe, increase the chances that a cortical cell that receives inputs from both of these TC cells will be able to discriminate the input as arising from different sectors of the sensory environment (e.g. whiskers).

With no electrical synapse between the pairs, the inhibitory feedback from TRN to TC cells is the sole influence that acts to separate spike trains for our inputs, and thus the inputs that TC relays to cortex (Fig. 1B). More specifically, increases in inhibitory strength between TRN and TC cells result in earlier termination of spiking in the TC cells (Fig. 1B–D). This resulted in increases in both separation, starting from trains that overlapped by −32 ms at $G_{GABA} = 0$ to a separation of 9.5 ms at $G_{GABA} = 0.05$ mS/cm^2, and increases in independence (43 to 100% over the range of G_{GABA}) of the trains from each other (Fig. 1E). However, the spike times of TCs themselves remain unchanged in this case.

For increases in strength of the electrical synapse between TRN cells, we observed three effects that ultimately impacted the separation and independence of TC spiking in our simulations: latency of spiking in the TC that received inputs later, truncation of spike trains, and prevention of any spiking.

An example of electrical synapse-mediated changes in latency is shown in Fig. 2. In this case, input was delivered 40 ms to TC_2 after the input to TC_1, and both inputs were of the same strength (0.06 mS/cm^2). Inhibitory strength between TRN and TC cells was relatively low in this example simulation ($G_{GABA} = 0.02$ mS/cm^2). While the spike trains are always independent in this set of simulations, the initial separation (without electrical synapses) is 9.2 ms (Fig. 2A$_i$), and we note that a cortical neuron that receives and sums input trains from both TC_1

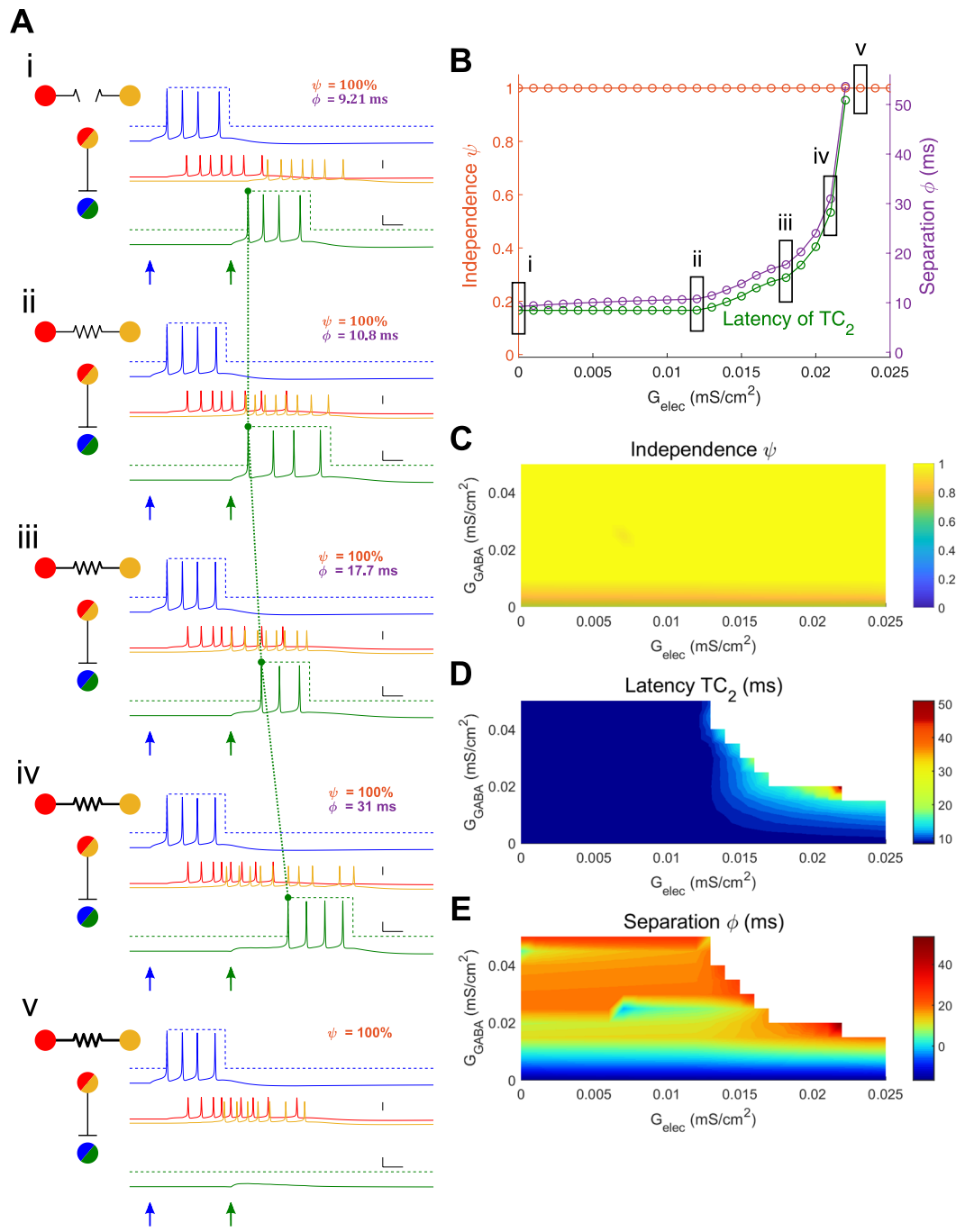

Figure 2. Electrical synapses between TRN cells result increase latency of TC spiking. (**A**) Example simulations with superimposed TC spiking windows. Input to TC_1 was constant (0.06 mS/cm^2, 60 ms). For these cases, input to TC_2 was 0.06 mS/cm^2, 100 ms, and inhibitory synapses were $G_{GABA} = 0.020$ mS/cm^2. Subpanels *i* – *v* show simulations with increasing electrical synapse strengths ($G_{elec} = 0$, 0.012, 0.018, 0.021, 0.023 mS/cm^2 respectively); for v, separation is undefined because at least TC_2 does not spike. (**B**) Independence (orange), separation (purple) and TC_2 latency (green) for simulations in A, over all values of electrical synapse strength. Latency of TC_2 has the same axis as separation. (**C**,**D**,**E**) Heat maps for independence, TC_2 latency, separation respectively against G_{elec} and G_{GABA}. Whitespace in latency indicates no spiking in TC_2 while blank space in separation means there is no spiking in either TC cell.

and TC_2 may not differentiate between one spike train that starts 9.2 ms after the termination of the previous train. Increases in electrical synapse strength within the model resulted in systematically delayed spiking of TC_2 from its input, from 8.5 to 51 ms (Fig. 2A$_{i–iv}$) with corresponding increases in separation between trains up to 55 ms (Fig. 2A$_{iv}$), and ultimately acted to prevent spiking in TC_2 (Fig. 2A$_v$). In these cases, separation values follow spike latencies and show a strong dependence on both electrical and inhibitory synapse strengths (Fig. 2B,D). We note that electrical synapse strength acts synergistically with inhibitory synapse strength (Fig. 2E), such that increases

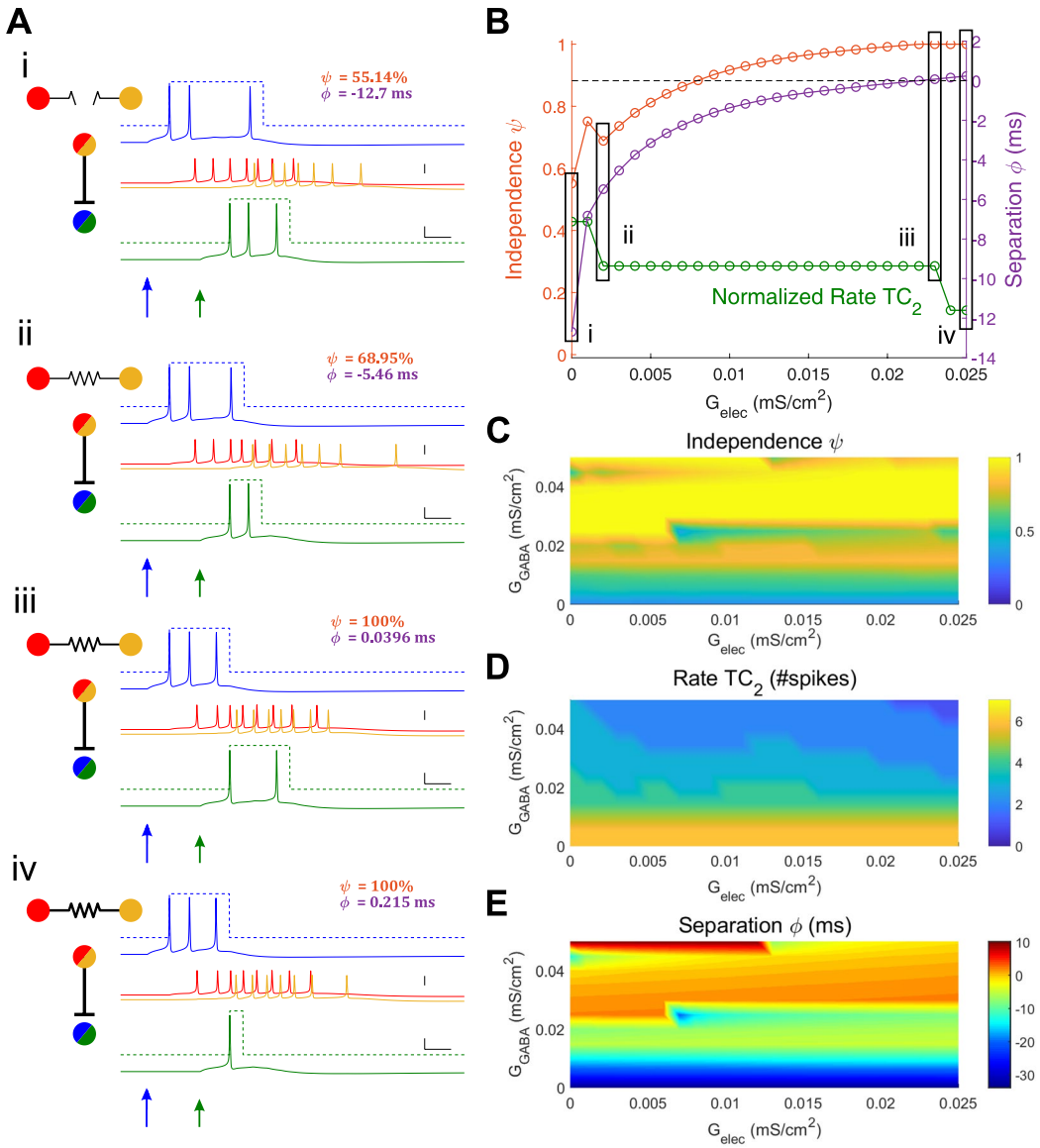

Figure 3. Electrical synapses between TRN cells result in truncated TC spike trains. (**A**) Example simulated traces. Input to TC_1 was constant (0.06 mS/cm^2, 60 ms). For these cases, input to TC_2 was 0.05 mS/cm^2, 80 ms and inhibitory synapses were $G_{GABA} = 0.045$ mS/cm^2; Subpanels *i* – *iv* show simulations with increasing electrical synapse strengths ($G_{elec} = 0$, 0.002, 0.023, 0.025 mS/cm^2 respectively). (**B**) Independence (orange), separation (purple) and normalized TC_2 rate (green) for the set of simulations in (**A**) plotted against electrical synapse strength. Normalized rate of TC_2 is the number of TC_2 spikes relative to the maximum over all simulations (7 spikes). (**C**,**D**,**E**) Heat map for independence, TC_2 rate (unnormalized), and separation respectively plotted against G_{elec} and G_{GABA}.

in both parameters result in large latency changes, or ultimately prevention of spiking in TC_2 (whitespace in Fig. 2D,E).

Spike train truncation arises for stronger values of inhibition within the network, and this effect modulated by the electrical synapse (Fig. 3). We illustrate this effect with a simulation in which a weaker (0.05 mS/cm^2) input was delivered to TC_2 20 ms after the input to TC_1. In this set, as electrical synapse strength increases, spiking in TC_2 decreases (Fig. 3A). Independence of the TC spike trains covaries with increases in electrical synapse strength, as the spike train of TC_2 diminish in spike count (Fig. 3D), and separation also increases (Fig. 3E). In this example, the baseline condition, with no or weak electrical synapses, is features moderately overlapping TC spike trains. However, the stronger inhibition in this example ($G_{GABA} = 0.045$ mS/cm^2) acts in concert with increasing values of electrical synapse strength to terminate any prolonged spiking of TC_2, from an initial 3 spikes to 1 spike (Fig. $3A_{i-iii}$), effectively decreasing overlap to eventually result in complete independence (from 55 to 100%) and increases in separation (−12.7 to 0.2 ms). For varied values of inhibitory strength within the network,

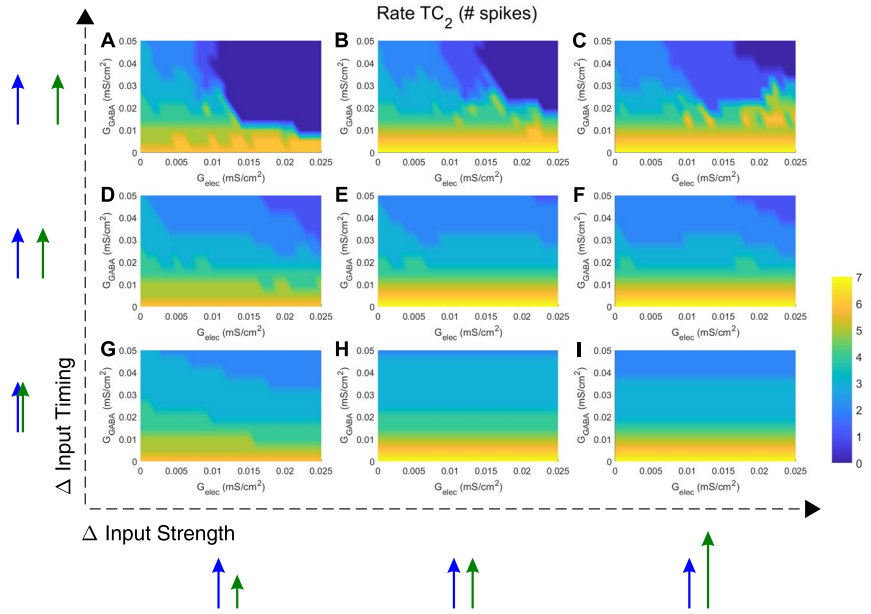

Figure 4. Electrical synapses between TRN cells modulate rate of TC_2. Each panel (**A**–**I**) is a heat map for TC_2 rate, plotted against all values of G_{elec} and G_{GABA}. Input strengths to TC_2 were varied between panels from left to right ($G_{in2} = 0.04$, 0.06 and 0.08 mS/cm^2; input to TC_1 was always $G_{in1} = 0.06$ mS/cm^2), and input timing was varied from bottom to top ($t_{in2} = 60$, 80 and 100 ms; t_{in1} was always 60 ms).

the relationships between independence, separation and electrical synapses become more complex, resulting from the dependence of rate (Fig. 3D) on both electrical and inhibitory synapse strength.

In general, spiking rate in TC_2 depends on both inhibitory and electrical synapse strength, as well as on the details of the input, specifically on its arrival time and strength. The dependence of spiking rate in TC_2 on electrical and inhibitory synapse strength is shown in Fig. 4. Generally, we see that electrical synapses between TRN cells are more effective in terminating trains for more temporally separated inputs (Fig. 4A–C), and require a minimal amount of electrical coupling ($G_{elec} > 0.01$) and inhibitory coupling ($G_{GABA} > 0.015$ mS/cm^2) to separate those inputs. The delays for input integration in TRN cells and TC cells determine the timescale at which electrical synapses influence the circuit. On the other hand, when inputs arrive more closely timed (Fig. 4G–I) and are more similar in strength (Fig. 4H), it takes both higher G_{elec} and G_{GABA} to cause any effects. In other words, the more different the inputs are, either in time or amplitude, the larger the effects are from the electrical and/or the inhibitory synapse.

Beyond spike number, electrical and inhibitory synapses also act together to regulate spike train separation (Fig. 5). Similar to the case for spiking rate, inputs arriving at the same time lead to overlapping TC spiking even for maximal electrical coupling and feedback inhibition (Fig. 5G–I), and the biggest impact of electrical synapses on separation is seen for inputs that are different in arrival time (Fig. 5A–C). Interestingly, weaker inputs require less inhibitory strength for the electrical synapse to increase temporal separation (Fig. 5A,D,G), and can prevent spiking when the inputs are far enough apart in time (Fig. 5A). This is a result of increased thalamocortical spiking delay, which results in larger separation values, and more time for weak or medium inhibition to act through electrical synapse and exert effects on the other TC cell.

For closely timed and similar inputs, electrical synapses are relatively ineffective in separating the inputs; in fact, for similar inputs, we observed that electrical synapses, acting through inhibitory synapses, instead result in temporal fusion of the inputs. This effect is shown in the progressive decrease in independence, indicated by the increased area of blue shading across sets of panels, in Fig. 6, where the center of each panel represents inputs of identical size and arrival time. Increases in electrical synapse strength, in this context, broaden the set of input differences for which spike trains are non-independent, seen when comparing sets of panels within Fig. 6. (% $\psi < 0.8$ increases from 32 to 46%), Fig. 6C (29 to 35%), and Fig. 6D (21 to 33%).

Finally, we evaluated the net gain in independence and separation created by the presence and strength of electrical synapses within the circuit over all values of G_{elec} and G_{GABA} used in our simulations. Here, we use radius of each concentric circle to represent a normalized combination of input strength and timing differences (Fig. 7). Identical inputs are thus at the center of each subpanel. In Fig. 8, each subpanel shows the difference in spike train independence or separation between that set of simulations (each subpanel represents a fixed pair of G_{GABA} and G_{elec}) and the baseline set of simulations, in which electrical synapses are absent. Finally, we separated gains in values, shown in the upper halves of each circle, and decreases in values, which are shown in the lower half.

From this figure, we see that as electrical synapse strength is increased (left to right), the gains in independence (Fig. 8A) and separation (Fig. 8B) from baseline of spike trains in the two TC cells can both increase or decrease (green or blue). Overall, we observe that there is an interaction between the strength of electrical and inhibitory synapses, where for each increase in G_{GABA}, a larger value of G_{elec} is necessary to influence the ultimate

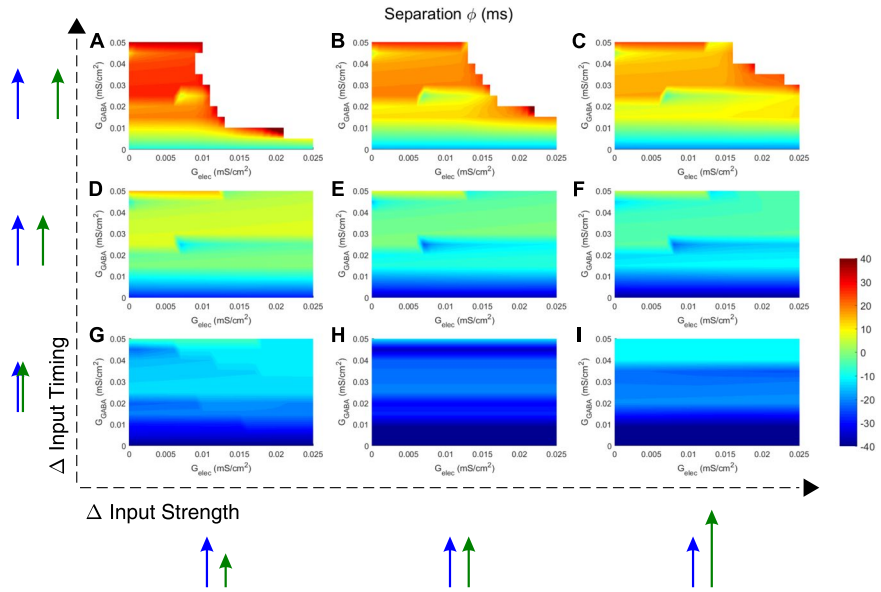

Figure 5. Electrical synapses between TRN cells increase separation of TC spike trains. Each panel (**A**–**I**) is a heat map for separation between TC spike trains, plotted against all values of G_{elec} and G_{GABA}. Input strengths to TC_2 were varied between panels from left to right ($G_{in2} = 0.04$, 0.06 and 0.08 mS/cm^2; input to TC_1 was always $G_{in1} = 0.06$ mS/cm^2), and input timing was varied from bottom to top ($t_{in2} = 60$, 80 and 100 ms; t_{in1} was always 60 ms). Whitespace in separation means there is no spiking in either TC cell.

independence or separation of TC spike trains. This effect reflects the circuitry, in which the effects of the electrical synapse are imparted through the actions of the inhibitory synapses. For small values of G_{GABA}, increases in TC independence dominate the results, while for larger values of G_{GABA}, decreases become the more dominant effect. As above, effects (increase or decrease) are larger for larger radius, such that inputs with more differences are modified by the electrical synapses.

Changes in separation follow a similar trend. For each value of $G_{GABA,}$ as electrical synapse strength increases within the circuit, gains in separation become larger, especially for more-different inputs (larger radii). Thus the presence or increase in the electrical synapse acts to separate TC spike trains, and with that the possibility for the cortex to discriminate between them.

Discussion

Noting that most of the experimental demonstrations or computational simulations of circuits containing electrical synapses focus on the relationship between electrical synapses and synchrony, we set out to explore the impact of electrical synapses on transient spike train processing. Using a minimal 4-cell model of paired thalamic relay and thalamic reticular nucleus cells with a single electrical synapse to connect the pairs, here we have shown that through feedback inhibition, electrical synapses of the TRN influence both timing and rate of thalamic spiking. Ultimately, the electrical synapses of the TRN modulate both the temporal independence and separation of the spike trains that thalamic cells send on to cortex, thus impacting whether cortical cells receive spike trains that can be discriminated as arising from separate sensory receptors or receptive fields of the sensory surround.

The results of our simulations are important in the context of plasticity of electrical synapses in the TRN[23,24]. Our results show that changes in strength of electrical synapses can shift the character of a relay response, from one that separates its inputs to one that fuses inputs, for instance. Changes in the strength of electrical synapses are represented here by a shift along an axis, and show that even smaller changes in electrical synapse strength, such as the ~15% changes measured as a result of synchronized burst firing in TRN, have the potential to determine output rate, timing, independence and separation.

Changes in separation, latency and rate due to embedded electrical synapses within the thalamic relay circuitry might also increase efficient coding, by modulating the sparsity of sensory relay. Decorrelation in lateral geniculate nucleus[25] and retinal ganglion neuronal activity[26] in response to naturalistic stimulation, while additional correlation for white noise stimuli is achieved, is believed to improve sparse coding in the visual system and is predicted to be driven by the presence of inhibitory interneurons[27,28]. Additionally, it is worth noting that sparseness is not only formed spatially (a few active neurons in a population), but also temporally (involving restricted amount of spiking of active neurons)[29]. Modulation of separation and rate may affect not only sparsity in the relay system, but also on cortical neurons (or any higher order neuronal structures) via postsynaptic summation effects.

Our model is the simplest core unit, or motif, of intrathalamic connectivity, and our model assumed these four cells to be identical in term of intrinsic properties. Our motif of two coupled TC-TRN pairs further shows that electrical synapse not only affects thalamocortical rates and latencies, thus contributing to basic coding of spatial-temporal sensory inputs (for example, whisker inputs[4,5]), but also regulates temporal independence and separation. However,

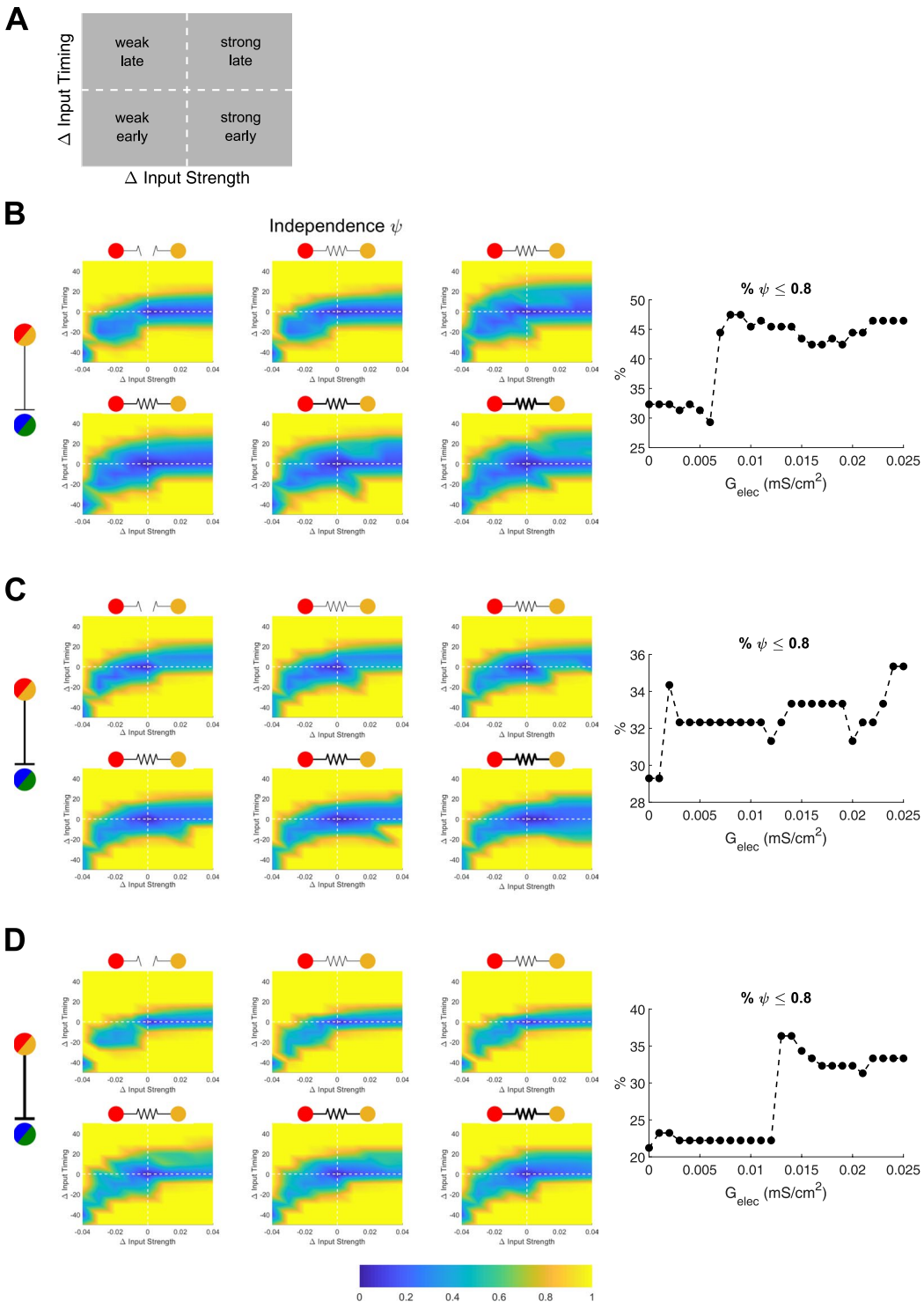

Figure 6. Electrical synapses between TRN cells merge TC spike trains for inputs that are similar in timing and strength. (**A**) Display convention for the following results, plotted by the differences of inputs to TC_2 in arrival time and strength relative to the fixed input to TC_1. The horizontal and vertical dashed lines represent simultaneous and equal inputs, respectively. (**B**,**C**,**D**) Independence plotted for varied values of electrical synapse strength and GABAergic inhibition ($G_{GABA} = 0.025$ in **B**, 0.040 in **C**, 0.050 mS/cm^2 in **D**), and the percent of simulations that resulted in independence (defined as $\Psi < 0.8$) plotted against electrical synapse strength for each set of simulations. The electrical synapse strength is indicated by thickness of symbol ($G_{elec} = 0$, 0.005, 0.010, 0.015, 0.020, 0.025 mS/cm^2).

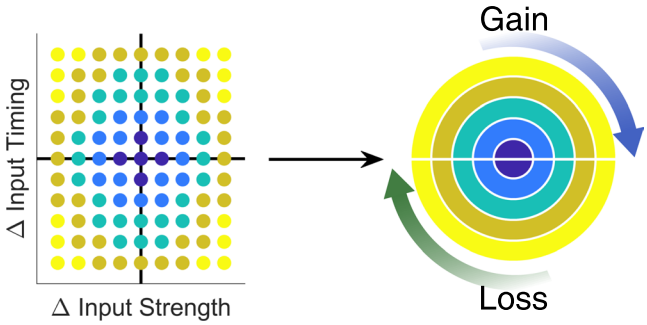

Figure 7. Mapping of normalized combination of input differences. Left: Input difference space, similar to that shown in Fig. 6A, with the black horizontal line representing inputs arriving simultaneously ($t_{in1} = t_{in2}$) and the black vertical line representing inputs of equal strength ($G_{in1} = G_{in2}$). Colors represent the 5 different strata of normalized combinations used to construct Fig. 8, with the darkest blue being the least different and yellow being the most different.

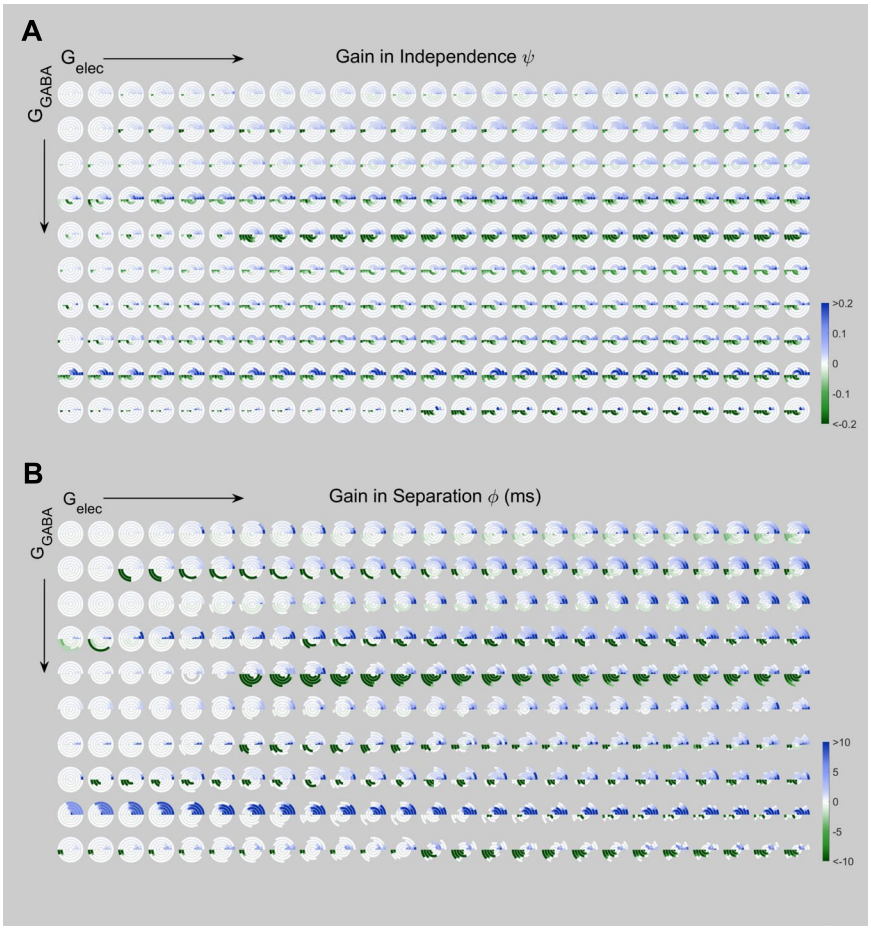

Figure 8. Change in spiking independence and separation between the two TC cells relative to uncoupled baseline (Gelec = 0). Each circle represents the difference of TC spike train independence or similarity, computed between results of simulations with $G_{elec} > 0$ (one set per panel) and the uncoupled case ($G_{elec} = 0$). From left to right, electrical synapse conductance increases across panels ($G_{elec} = 0.001$ to $0.025\ mS/cm^2$). From top to bottom, inhibitory synapse conductance increases ($G_{GABA} = 0.005$ to $0.050\ mS/cm^2$). Within each circle, radius represents input timing and strength similarity in 5 different strata, with the inner arcs representing the inputs to the two TC cells that were most similar in timing and strength, and outer arcs representing inputs that were most different (Fig. 8). Gains (blue hues) in TC spike train independence or separation are shown in the upper semicircle, and losses (green hues) in the lower semicircle (**A**) Gains or losses in spike train independence. (**B**) Gain or loss of spike train similarity; missing values (see Methods) are represented as having no color.

connections within thalamus and between thalamus and cortex are more substantially complex *in vivo*. Thalamic cells receive convergent inhibitory inputs from multiple TRN cells, and TRN cells receive input from multiple thalamic relay cells. While we have focused on straightforward thalamic relay of singular inputs, mimicking POm, other thalamic subsectors receive inputs from broad areas of the sensory surround. Cortical feedback is also not represented in the present model, and neuromodulation is also unaccounted for. Thus, there is much future work to be done to thoroughly explore the role of electrical synapses in transient signal processing within thalamus.

The underlying circuit – inhibitory neurons connected by an electrical synapse, and providing feedback inhibition to the principal neurons that excite them – is one that we expect may be embedded within retina, where AII amacrine cells regulate retinal ganglion cell spiking; and within cortex, where inhibitory neurons regulate principal cell firing, as well as in the cerebellum. We expect that the general principles seen here – that electrical synapses act through inhibitory synapses to increase latency, decrease spike rates, and modify the independence and separation of spike trains in principal cells – will also impact information processing in the many areas that contain electrical synapses.

Our results make specific predictions that can be tested in experiments. For example, we predict that the spiking responses of nearby PoM neurons with overlapping receptive fields to peri-threshold inputs will be modulated by either altering or abolishing electrical synaptic strength in TRN by electrical[24], pharmacological[30,31] or optogenetic means. We expect to see, especially in cases of separated input arrival timings that potentiated electrical coupling leads to decreased spiking and increased separation, while depressed or blocked electrical coupling leads to increased spiking and decreased separation.

References

1. Alloway, K. D. Information processing streams in rodent barrel cortex: the differential functions of barrel and septal circuits. *Cereb Cortex* **18**, 979–989, https://doi.org/10.1093/cercor/bhm138 (2008).
2. Harris, R. M. Axon collaterals in the thalamic reticular nucleus from thalamocortical neurons of the rat ventrobasal thalamus. *J Comp Neurol* **258**, 397–406, https://doi.org/10.1002/cne.902580308 (1987).
3. Sherman, S. M. & Guillery, R. W. Functional organization of thalamocortical relays. *J Neurophysiol* **76**, 1367–1395 (1996).
4. Yu, C. *et al*. Coding of object location in the vibrissal thalamocortical system. *Cereb Cortex* **25**, 563–577, https://doi.org/10.1093/cercor/bht241 (2015).
5. Sosnik, R., Haidarliu, S. & Ahissar, E. Temporal frequency of whisker movement. I. Representations in brain stem and thalamus. *J Neurophysiol* **86**, 339–353 (2001).
6. Houser, C. R., Vaughn, J. E., Barber, R. P. & Roberts, E. GABA neurons are the major cell type of the nucleus reticularis thalami. *Brain Res* **200**, 341–354 (1980).
7. Pinault, D. & Deschenes, M. Projection and innervation patterns of individual thalamic reticular axons in the thalamus of the adult rat: a three-dimensional, graphic, and morphometric analysis. *J Comp Neurol* **391**, 180–203 (1998).
8. Gentet, L. J. & Ulrich, D. Strong, reliable and precise synaptic connections between thalamic relay cells and neurones of the nucleus reticularis in juvenile rats. *J Physiol* **546**, 801–811 (2003).
9. Ohara, P. T. & Lieberman, A. R. The thalamic reticular nucleus of the adult rat: experimental anatomical studies. *J Neurocytol* **14**, 365–411 (1985).
10. Shosaku, A. Cross-correlation analysis of a recurrent inhibitory circuit in the rat thalamus. *J Neurophysiol* **55**, 1030–1043 (1986).
11. Mayer, J., Schuster, H. G. & Claussen, J. C. Role of inhibitory feedback for information processing in thalamocortical circuits. *Phys Rev E Stat Nonlin Soft Matter Phys* **73**, 031908, https://doi.org/10.1103/PhysRevE.73.031908 (2006).
12. Le Masson, G., Renaud-Le Masson, S., Debay, D. & Bal, T. Feedback inhibition controls spike transfer in hybrid thalamic circuits. *Nature* **417**, 854–858, https://doi.org/10.1038/nature00825 (2002).
13. Hou, G., Smith, A. G. & Zhang, Z. W. Lack of Intrinsic GABAergic Connections in the Thalamic Reticular Nucleus of the Mouse. *J Neurosci* **36**, 7246–7252, https://doi.org/10.1523/JNEUROSCI.0607-16.2016 (2016).
14. Landisman, C. E. *et al*. Electrical synapses in the thalamic reticular nucleus. *J Neurosci* **22**, 1002–1009 (2002).
15. Connors, B. W. & Long, M. A. Electrical synapses in the mammalian brain. *Annu Rev Neurosci* **27**, 393–418 (2004).
16. Gutierrez, G. J., O'Leary, T. & Marder, E. Multiple mechanisms switch an electrically coupled, synaptically inhibited neuron between competing rhythmic oscillators. *Neuron* **77**, 845–858, https://doi.org/10.1016/j.neuron.2013.01.016 (2013).
17. Pfeuty, B., Mato, G., Golomb, D. & Hansel, D. The combined effects of inhibitory and electrical synapses in synchrony. *Neural Comput* **17**, 633–670 (2005).
18. Lewis, T. J. & Rinzel, J. Dynamics of spiking neurons connected by both inhibitory and electrical coupling. *J Comput Neurosci* **14**, 283–309 (2003).
19. Lewis, L. D. *et al*. Thalamic reticular nucleus induces fast and local modulation of arousal state. *Elife* **4**, e08760, https://doi.org/10.7554/eLife.08760 (2015).
20. Fogerson, P. M. & Huguenard, J. R. Tapping the Brakes: Cellular and Synaptic Mechanisms that Regulate Thalamic Oscillations. *Neuron* **92**, 687–704, https://doi.org/10.1016/j.neuron.2016.10.024 (2016).
21. Destexhe, A., Bal, T., McCormick, D. A. & Sejnowski, T. J. Ionic mechanisms underlying synchronized oscillations and propagating waves in a model of ferret thalamic slices. *J Neurophysiol* **76**, 2049–2070 (1996).
22. Traub, R. D. *et al*. Single-column thalamocortical network model exhibiting gamma oscillations, sleep spindles, and epileptogenic bursts. *J Neurophysiol* **93**, 2194–2232, https://doi.org/10.1152/jn.00983.2004 (2005).
23. Haas, J. S., Zavala, B. & Landisman, C. E. Activity-dependent long-term depression of electrical synapses. *Science* **334**, 389–393 (2011).
24. Landisman, C. E. & Connors, B. W. Long-term modulation of electrical synapses in the mammalian thalamus. *Science* **310**, 1809–1813 (2005).
25. Dan, Y., Atick, J. J. & Reid, R. C. Efficient coding of natural scenes in the lateral geniculate nucleus: experimental test of a computational theory. *J Neurosci* **16**, 3351–3362 (1996).
26. Pitkow, X. & Meister, M. Decorrelation and efficient coding by retinal ganglion cells. *Nat Neurosci* **15**, 628–635, https://doi.org/10.1038/nn.3064 (2012).
27. Vinje, W. E. & Gallant, J. L. Sparse coding and decorrelation in primary visual cortex during natural vision. *Science* **287**, 1273–1276 (2000).
28. King, P. D., Zylberberg, J. & DeWeese, M. R. Inhibitory interneurons decorrelate excitatory cells to drive sparse code formation in a spiking model of V1. *J Neurosci* **33**, 5475–5485, https://doi.org/10.1523/JNEUROSCI.4188-12.2013 (2013).
29. Kloppenburg, P. & Nawrot, M. P. Neural coding: sparse but on time. *Curr Biol* **24**, R957–959, https://doi.org/10.1016/j.cub.2014.08.041 (2014).
30. Wang, Z., Neely, R. & Landisman, C. E. Activation of Group I and Group II Metabotropic Glutamate Receptors Causes LTD and LTP of Electrical Synapses in the Rat Thalamic Reticular Nucleus. *J Neurosci* **35**, 7616–7625 (2015).
31. Sevetson, J., Fittro, S., Heckman, E. & Haas, J. S. A calcium-dependent pathway underlies activity-dependent plasticity of electrical synapses in the thalamic reticular nucleus. *The Journal of Physiology*, n/a-n/a, https://doi.org/10.1113/JP274049 (2017).

Acknowledgements
This work was supported by the Whitehall Foundation and NSF IOS 1557474 to JSH.

Author Contributions
T.P. and J.S.H. planned simulations. T.P. executed simulations and performed data analysis. T.P. and J.S.H. prepared figures and wrote the manuscript.

Additional Information
Competing Interests: The authors declare no competing interests.

Publisher's note: Springer Nature remains neutral with regard to jurisdictional claims in published maps and institutional affiliations.

Open Access This article is licensed under a Creative Commons Attribution 4.0 International License, which permits use, sharing, adaptation, distribution and reproduction in any medium or format, as long as you give appropriate credit to the original author(s) and the source, provide a link to the Creative Commons license, and indicate if changes were made. The images or other third party material in this article are included in the article's Creative Commons license, unless indicated otherwise in a credit line to the material. If material is not included in the article's Creative Commons license and your intended use is not permitted by statutory regulation or exceeds the permitted use, you will need to obtain permission directly from the copyright holder. To view a copy of this license, visit http://creativecommons.org/licenses/by/4.0/.

© The Author(s) 2018